Electron-Transfer Emission Spectra of a Cyanide-Bridged, Cr(III)/Ru(II) Donor−Acceptor Complex: High Frequency (N−H and C≡N) Vibronic Contributions from Empirical Reorganizational Energy Profiles

Yuan-Jang Chen, Puhui Xie, and John F. Endicott*

Department of Chemistry, Wayne State University, Detroit, Michigan 48202-3929

Received: January 15, 2004; In Final Form: March 15, 2004

The resolution of the contributions of CN and NH vibronic sidebands to the 77 K, transition metal-to-transition metal electron-transfer (MMCT) emission for a cyanide-bridged Ru(II)/Cr(III) coordination complex is reported. These vibronic sidebands were identified, and their reorganizational energy contributions evaluated by comparing the reorganizational energy profiles of the proteo (NH) and deutereo (ND) am(m)ine complexes in glassy solutions and in the microcrystalline solid. The reorganizational energy profiles were generated by subtracting a gaussian fit of the dominant, fundamental emission component ($h\nu_{0'0(\max)} = 12\,050$ cm^{-1} in glasses; 12 400 cm^{-1} in the solid) from the high resolution, near-infrared emission spectrum, scaling the remainder amplitudes so that they correspond to the sum of reorganizational energy contributions at each emission energy and correcting for the effects of the significant component bandwidths. The reorganizational energy attributable to the NH-stretch in DMSO/water glasses, $\lambda_{NH} \cong 28 \pm 5$ cm^{-1}, is much smaller than the values of $\lambda_x = 200-400$ cm^{-1} attributable to the lower frequency vibrations (the dominant distortion modes; probably metal−ligand skeletal vibrations and C≡N stretches). There also appears to be a similarly small contribution to the reorganizational energy from NH_2 bending modes. The value of λ_{NH} is consistent with a tunneling pathway for the back electron-transfer and with the very large NH/ND isotope effect observed for this complex. The reorganizational energy contribution attributable to the CN stretching vibration of the bridging ligand is greater than 100 cm^{-1}. The molecular reorganizational contributions for the back electron-transfer are 30−40% smaller in butyronitrile glasses than in DMSO/water glasses or in the solid. This may be a consequence of configurational (or intervalence) mixing of the MMCT excited state with the ligand field ^{2}E excited state of the chromium center.

Introduction

Transition metal-to-transition metal electron-transfer (here designated, MMCT) emission spectra are very rare. To our knowledge, the only report of such spectra is a preliminary report from this laboratory.[1] We have now obtained much higher quality, near-infrared emission spectra, over a much-extended wavelength range of a cyanide-bridged ruthenium/chromium, donor/acceptor complex at 77 K. Electron-transfer emission spectroscopy can, in principle, provide unique information about the factors that govern the transitions between electron-transfer states.[2−4] In particular, the vibronic components of the emission spectrum can be related to the Franck−Condon factor of the electron-transfer rate constant. An important feature of these MMCT emissions is the very large increase in the 77 K excited-state lifetimes upon am(m)ine perdeuteration: values of $k_{NH}/k_{ND} = 15-30$ increase with the number of am(m)ine moieties. This implicates a NH-mediated nuclear tunneling pathway for the 77 K back electron-transfer. The high-frequency vibronic components are important in determining the magnitude of the nuclear tunneling contribution to the limiting low-temperature rate constant. It has been very difficult to obtain information about these vibronic contributions to emission spectra because they are weak and displaced to energies 2000−3000 cm^{-1} lower than that of the emission maximum (about 12 000 cm^{-1} for the compound considered here). In this study of a MMCT emission, we have been able to resolve, for the first time, and to evaluate the reorganizational energy contributions of vibronic components attributable to the N−H stretch of am(m)ine ligands coordinated to transition metal chromophores.

The irradiation of the MMCT absorption band of [Cr([14]-aneN$_4$)(CNRu(NH$_3$)$_5$)$_2$]$^{5+}$ (see Figure 1) in ambient solution produces a transient species with a 7 ns lifetime that is consistent with an electron-transfer excited state.[5,6] Estimates of the pertinent Franck−Condon parameters imply that the back electron-transfer falls in the Marcus inverted region,[1,6] and this is confirmed by the 77 K MMCT emission.[1] The rate constants for the back electron-transfer processes (or the inverse mean lifetimes of electron-transfer excited states) are functions of the initial state-final state energy difference, $E_{ge}^{0'0}$, the differences in the nuclear coordinates in the two states and the electronic coupling between the states.[3,4,7−19] The relative importance of different nuclear coordinates (i.e., the displacements of nuclei that correlate with the differences in the geometries and solvation of the initial and final states) has been difficult to establish for electron transfer processes of transition metal complexes in the Marcus inverted region. A variety of properties of these complexes have made this difficult: (a) the relatively small energy differences between electronic states[20] often complicate studies based on absorption spectroscopy; (b) there are many low-frequency molecular vibrational modes that might contribute;[21] and (c) perhaps most importantly, electron-transfer

* To whom correspondence should be addressed. E-mail: jfe@chem.wayne.edu.

10.1021/jp0497817 CCC: $27.50
Published on Web 05/15/2004

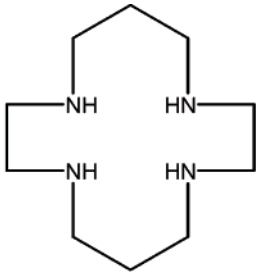

[14]aneN$_4$ (cyclam)

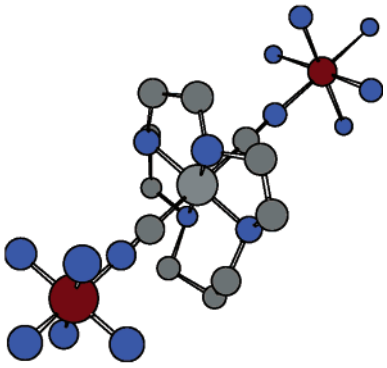

[Cr([14]aneN$_4$)(CNRu(NH$_3$)$_5$)$_2$]$^{5+}$

Figure 1. Skeletal structures of the [14]aneN$_4$ tetraazamacrocyclic ligand and of the [Cr([14]aneN$_4$)(CNRu(NH$_3$)$_5$)$_2$]$^{5+}$ complex. Hydrogen atoms have been omitted for clarity.

emission spectra of transition metal donor/acceptor (D/A) complexes are very rare.[1]

Emission spectra are relatively well suited for this purpose since they almost always correspond to transitions between two well-defined electronic states, whereas the information provided by other spectroscopic probes is often complicated by the convoluted contributions of several different electronic states.[22] The vibronic components of the distortion modes, $h\nu_h \geq 4k_BT$, associated with the Franck−Condon factors of electron-transfer processes are best resolved at low temperatures where the component bandwidths are relatively small. One expects that the molecular distortions will be largely independent of temperature, solvent, or other environmental factors. The intensities of the first vibronic components of each vibronic progression, $I_{0'1}(h)$, relative to the intensity of the fundamental, $I_{0'0}$, is equal to the reorganizational energy component for that mode, λ_h (proportional to the square of the displacement of excited state along the ν_h mode), divided by $h\nu_h$[23,24]

$$\frac{I_{0'1}(h)}{I_{0'0}} = \frac{\lambda_h}{h\nu_h} \qquad (1)$$

At sufficiently low temperatures, thermally activated, nonradiative relaxation will be unimportant and nuclear tunneling pathways for excited state relaxation will be correspondingly more important.[14,15,25] Although nuclear tunneling is expected to be dominated by the highest frequency vibrational modes, which are not necessarily the dominant displacement modes, only modes that correspond to some excited-state displacement can be important in mediating tunneling.[14,15] Consequently, the dominant tunneling modes should exhibit a corresponding vibronic component in the emission spectrum. However, eq 1 indicates that the emission intensities of such components may be very weak. The N−H stretching modes, with $h\nu_h \sim 2800-3200$ cm^{-1}, are the highest frequency vibrational modes in transition metal am(m)ine complexes. The MMCT emission spectra reported here have permitted us to evaluate the contributions of the N−H stretching modes.

The very large isotope effects in the series of complexes clearly implicate an NH-mediated nuclear tunneling pathway for back electron-transfer in these complexes. Partly for reasons of their relatively low energies and large vibrational frequencies (resulting in small intensities; eq 1), there have been few or no reports on NH vibrational sidebands in the emission spectra of transition metal complexes. To facilitate our search for these high-frequency vibronic components, we have presented the spectroscopic observations in a way that emphasizes the reorganizational energy contributions by means of rescaling the emission intensity based on $\lambda_h = I_{obsd}(h\nu_h/I_{0'0})$ from eq 1. This makes the contributions of the high-frequency vibronic components to the experimental spectra much easier to identify.

Experimental Section

(a) Materials and Experimental Techniques. The synthesis and characterization of *trans*-bis(pentaammineruthenium(II)-μ-isocyano)(1,4,8,11-tetraazacyclotetradecane)chromium(III), [Cr([14]aneN$_4$)(CNRu(NH$_3$)$_5$)$_2$]$^{5+}$ has been described previously.[26−28] The skeletal structures of the complex and the tetraazamacrocyclic ligand are illustrated in Figure 1. Deuteration of the am(m)ine moieties of the complexes was performed by means of exchange of the complex in D_2O solutions in an argon atmosphere in a glovebag. The solvents used were spectral grade.

Absorption spectra were obtained using a Shimadzu UV 2101PC spectrophotometer.

Luminescence lifetimes were determined by collecting and focusing the emitted light onto an ISA H-100 monochromator attached to a Hammamatsu 955 PMT. The PMT signal was digitized with a LeCroy 9310 digital oscilloscope and transferred to a computer. Software for this system was written by OLIS, Inc. (Jefferson, GA). Samples were excited using a Molectron DL-14 dye laser pumped by a Molectron UV-1010 nitrogen laser. Typically, 300 shots were averaged for the lifetimes. The dye laser output wavelength was monitored by observing the second-order scattering of light from the laser using the InGaAs detector.

Emission spectra in 77 K glasses were obtained using a Princeton Instruments (Roper Scientific) OMA V InGaAs 512 pixel array detector mounted on an Acton SP500 spectrometer (wavelength calibration with respect to Xe emission lines and intensity calibration relative an Oriel model 63358 Quartz Tungsten Halogen QTH lamp with NIST traceable calibrated intensity). Emission measurements at 77 K were made using DMSO:H_2O (1:1), DMSO:D_2O (1:1), butyronitrile glasses or on the microcrystalline solid. The samples in 1 mm i.d. cylindrical quartz cells were immersed in liquid nitrogen in a spectroscopic quartz dewar, which was secured with a Derlin holder. Microcrystalline solid samples were prepared for emission studies by allowing solutions of the complexes to evaporate in the luminescence sample cells. The sample cell and Dewar were aligned for each experiment to optimize the signal. Optical filters were used to reduce the scattered laser light. The emission data were collected using a 300 g/mm grating, blazed at 1000 nm (effective observation window of 150 nm), and the WinSpec program operated in the scan-accumulate-paste mode. CW excitation was provided by MGL-S-B 50 mW (532 nm) diode laser modules (Changchun Industries Optoelectronics Tech Co. Ltd.) purchased from OnPoint Lasers, Inc. A dichroic mirror was used to reduce the long wavelength laser emissions.

(b) Spectral Deconvolutions and the Generation of Empirical Reorganizational Energy Profiles (emreps). ACSII files were transferred from the WinSpec program (controlling the emission spectrometer) to EXCEL then to Grams/32 for gaussian deconvolutions. The emission intensities were divided by the frequency of light emitted for these fits.[4,29] The principal feature of the emission spectrum was matched as closely as possible to a single gaussian component in its intensity and in the slope on its high energy side.[22] These components are assigned as the $[e,0'] \rightarrow [g,0]$ fundamentals of the emission bands ($j = 0$ in eqs 2−5). The remaining gaussian components were constructed as necessary to give a good fit ($R^2 > 0.995$) to the spectrum. The spectra were fitted using the smallest number of components that would give a good fit. This is illustrated for the emission spectrum of $[Cr([14]aneN_4)(CNRu(NH_3)_5)_2]^{5+}$ in Figure 2a.

The emission spectrum can be represented as in the equations below for a single high-frequency mode:[4,29−31]

$$I_{\nu m} = \frac{64\pi^4}{3h^3c^3 \ln 10} \frac{\nu_m \eta^3 H_{eg}{}^2 (\Delta\mu_{ge})^2}{(4\pi\lambda_l k_B T)^{1/2}} (FC) \qquad (2)$$

$$(FC) = \sum_h \sum_j F_{j,h} [e^{-(G_j)^2/(\Delta\nu_{1/2}{}^2/4\ln 2)}] \qquad (3)$$

$$F_{j,h} = S_h^j [\exp(-S_h)]/j! \qquad (4)$$

$$S_h = \lambda_h / h\nu_h$$

$$G_j = E_{ge}^{0'0} - \lambda_r - jh\nu_h - h\nu_{em} \qquad (5)$$

The components of (FC) are then gaussian functions whose full widths at half-height, $D\nu_{1/2}$, are the same as that of the fundamental (i.e., the function with $j = 0$)[2,32,33]

$$\Delta\nu_{1/2} = 4[k_B T \lambda_l \ln(2)]^{1/2} + \sigma \qquad (6)$$

Any low-frequency vibrational modes with $h\nu_l \leq 4k_B T$ will contribute to the bandwidth; other contributions, σ, may arise from the distribution of solvent environments of the emitting species in the frozen solutions,[34] quality of the glassy matrix, optical resolution, or other factors.

One can make the vibronic contributions more evident by subtracting the fitted Gaussian component, identified as the $[e,0'] \rightarrow [g,0]$ fundamental, from the observed spectrum, as illustrated in Figure 2b. However, the high-frequency contributions are still very weak in this difference spectrum.

We have rescaled the difference spectra, based on $\lambda_h = I_{obsd}(h\nu_h/I_{0'0})$, to emphasize the high-frequency vibronic contributions. The details are presented in Appendix A. The relative significance of the contributions of distortions in high-frequency modes is evident from the resulting emreps, as in the example in Figure 2c, since the amplitudes can be read as reorganizational energies

$$\lambda_x = h\nu_x [I_{obsd}(\nu_d) - I_{0'0}(\nu_d)]/I_{0'0}(\nu_{0'0(max)}) \qquad (7)$$

The emreps are generated by plotting λ_x vs $h\nu_x = h(2\nu_d - [\{\nu_d\}^2 + a^2]^{1/2})$, as shown in Appendix A.

Results

Good quality 77 K emission spectra were obtained with a Princeton Instruments OMA V InGaAs array detector using samples of the complexes dissolved in DMSO:H_2O, butyronitrile, or samples of the pure microcrystalline solid; there were differences in bandwidths (smallest in the solid, largest in the frozen solutions) and energies (highest in the solid). As noted previously,[1] the emission spectra of this complex broaden and shift to higher energies when the excitation energy is on the high energy side of the MMCT absorption ($\lambda_{max} \cong 500$ nm in ambient solution; Figure 3 and Table 1).[1] The emission spectra reported here are the narrowest that we have observed. The emission bandwidth was also significantly affected by the quality of the glass at 77 K. The glass quality was monitored visually for each spectral determination, and the spectral determinations

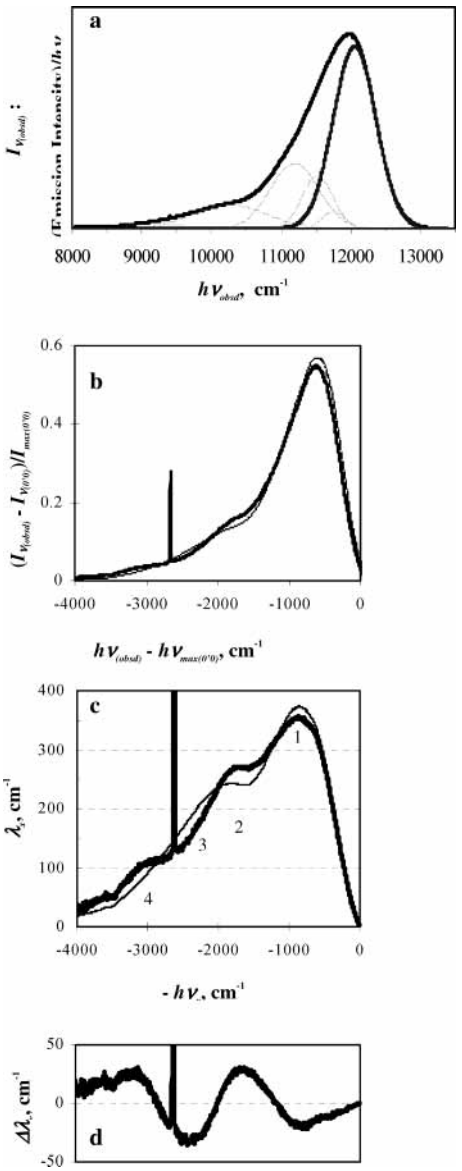

Figure 2. Steps in the identification of the 77 K emission band components of $[Cr([14]aneN_4)(CNRu(NH_3)_5)_2]^{5+}$ in DMSO/water: a. The MMCT emission spectrum (heavy lines); b. the difference between the observed spectrum and the fundamental for (CrCNRu(NH)), heavy line, and (CrCNRu(ND)), light line; c. the emperical reorganizational energy profiles of (CrCNRu(NH)),heavy line, and of (CrCNRu(ND)), light line; d. the difference of those profiles, bottom. The reorganizational energy profiles are derived from the emission spectra by using Equations A4 and 7 to construct the ordinate and abscissa, respectively. Vibrations of energy $h\nu_x$ can be associated with the reorganizational energy contributions (in cm^{-1}; tentative assignments in parentheses) in the ranges: 400−800 (metal−ligand stretch; M−N−H bend); 2, 1500−2000 (C≡N stretch; NH_2 bend); 3, 2100−2700 (N−D stretch); 4, 2900−3600 (N−H stretch).

TABLE 1: Ambient Absorption and 77 K Emission Parameters for the NH and ND Isotopomers of $[Cr([14]aneN_4)(CNRu(NH_3)_5)_2]^{5+}$

isotopomer[a]	matrix	absorption[b,c] $h\upsilon_{MMCT(max)}$, nm[cm^{-1}] ($\epsilon \times 10^{-3}$) {$h\upsilon_{0'0(max)}$, cm^{-1}} $\langle\Delta\upsilon_{1/2}\rangle$	emission $h\upsilon_{MMCT(max)}$	fundamental $h\upsilon_{0'0(max)}$ [$\Delta\upsilon_{1/2}$][f]	$h\upsilon_x$[c,d]	λ_x[c]	k_n[e]
NH	DMSO− H_2O	517[19300] (6.82) {19470} ⟨3690⟩	11990	12060[710]	430∼1000 1500∼2050 2800∼3500 ∼*3200(NH)* ∼1650(NH_2)	350 270 60−120 28 30	1.3
ND	DMSO− D_2O		11980	12060[720]	430∼1000 1500∼2050(CN) 2050∼2800 ∼2500(ND) ∼800	370 240 120∼230 30 20	0.094
NH	Butyronitrile	515[19400] (7.93) {19550} ⟨3510⟩	11980	12030[680]	590∼1000 1500∼2050 2800∼3500 ∼3200(NH) ∼1700(NH_2)	260 135 20−50 6 4	0.39
ND	Butyronitrile		11970	12040[720]	590∼1000 1500∼2050(CN) 2050∼2800 ∼2500(ND) ∼930	270 130 125−50 8 10	0.25
NH	Solid		12310	12390[650]	420∼1080 1480∼2030 3020∼4000 ∼3500(NH) ∼1560(NH_2)	410 270∼280 100−30 15 20	1.1
ND	Solid		12300	12410[610]	420∼1080 1530∼2050(CN) 2050∼2760 ∼2300(ND) ∼690	430 260 240−130 15 30	0.42

[a] NH = $[Cr([14]aneN_4)(CNRu(NH_3)_5)_2]^{5+}$; ND = $[Cr(d_4\text{-}[14]aneN_4)(CNRu(ND_3)_5)_2]^{5+}$. [b] Ambient aqueous solution. [c] All energy quantities in units of cm^{-1}. [d] Approximate range of contributions except for italicized entries. Entries based on the difference between isotopomer emreps are in italics; the energy of the maximum difference is noted. [e] Amplitude averaged emission decay rate constants in units of μs^{-1}. [f] Values of the energy maximum and Gaussian full width at half-height for the fundamental emission component.

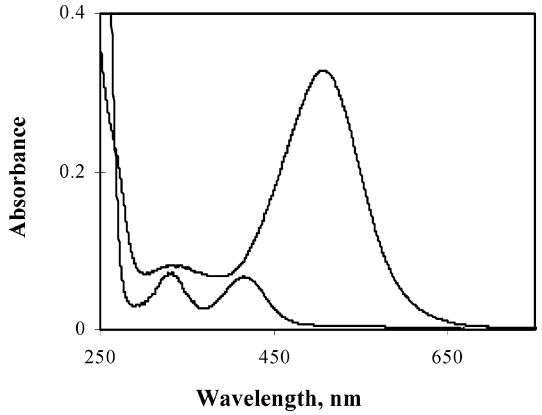

Figure 3. Visible absorption spectrum of $[Cr([14]aneN_4)(CNRu(NH_3)_5)_2]^{5+}$ (0.04 mM), upper curve, and $[Cr([14]aneN_4)(CN)_2]^{+}$ (1 mM), lower curve; in aqueous solution.

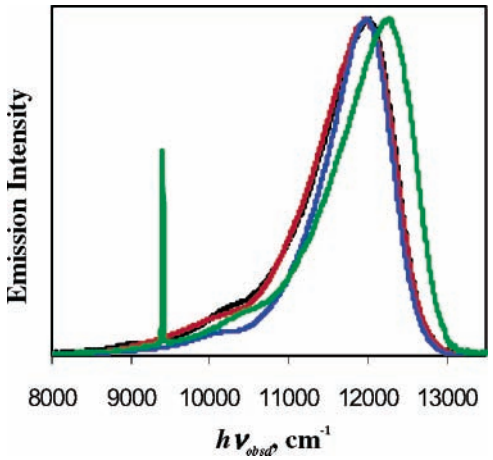

Figure 4. Emission spectra (77 K) of $[Cr([14]aneN_4)(CNRu(NH_3)_5)_2]^{5+}$ in $DMSO/H_2O$ (black curve), butyronitrile (blue curve), and microcrystalline solid (green curve); red curve for $[Cr(d_4\text{-}[14]aneN_4)(CNRu(ND_3)_5)_2]^{5+}$ in $DMSO/D_2O$. The sharp feature at 9398 cm^{-1} is scattered light (second order and/or fundamental) from the excitation laser.

were repeated many times with different solutions and 532 nm excitation sources to ensure reproducibility.

The 77 K emission spectra are presented in Figures 2 and 4. These spectra are broadened on the low energy side, consistent with unresolved contributions from relatively weak vibronic sidebands. To examine these vibronic contributions more critically, we have displayed the spectroscopic observations as emreps. These profiles assume that the emission spectrum can be represented as the sum over some set(s) of vibronic progressions (the components of a progression are designated by subscript *j*; different vibronic progressions by a subscript *h*; $E_{ge}^{0'0} > 0$ is the difference in zero point energies of the excited and ground state; see eqs 2−6). The profile amplitudes contain contributions from higher order vibronic components when $h\nu_x$ is large (greater than ∼ 600 cm^{-1}). The second-order term contributions to the reorganizational amplitudes at $2h\nu_x$ are of the order of $\sum_h(\lambda_h^2/h\nu_h)$; see eqs 2−6. Neither the first order nor second order vibronic components are well resolved in the emission spectrum or in the reorganizational energy profiles. This is most likely due to a combination of the finite bandwidths with the contributions of several high frequency vibrational modes that do not differ greatly in energy. For example, the principal contributions to the reorganizational energy profile are

expected to correspond to the energies of vibrations in the metal−ligand stretching region (Figure 2c). Even for the highest possible symmetry, D_{4h}, of the ground state of this complex (the actual maximum symmetry is C_{2h}), there are 15 nondegenerate metal−ligand stretching modes in the 350−650 cm^{-1} region.[35] One would expect that the largest changes in coordination sphere bond lengths would be associated with the formation of Cr^{II} from Cr^{III}, and these would be mostly in the $Cr-N_4$ equatorial plane; this would correspond to a minimum of three metal−ligand vibrational frequencies corresponding to the distortion modes (including one set of degenerate vibrations). The distribution of the reorganizational energy contributions over these modes would result in relatively small second-order contributions at any specific energy. Nevertheless, one does expect the sum of all of the second-order contributions to complicate the evaluation of the contributions of weak, high-frequency vibrational modes, in effect increasing the background noise as ν_x increases. For this reason we have made careful comparisons of the emreps of the proteo-am(m)ine (NH) and deutereo-am(m)ine (ND) complexes in order to resolve the reorganizational energy contributions of the NH vibrations.

The intensities of eq 1 refer to the integrated intensities over the respective component emission bands for a single high-frequency vibrational mode. The integrated intensity of a gaussian emission band is proportional to the intensity at the maximum times the bandwidth, the vibronic components all should have the same bandwidth, and the ratio of intensities at the component maxima is equal to the ratio of integrated intensities. The fundamental emission components have appreciable bandwidths in all media employed. The interpretation of the maximum contribution of a single distortion mode, ν_h, to the profile is embodied in eq 1, as noted above, but the interpretation of the envelope of the contributions of several modes with slightly different values of ν_h is not simple in either the difference spectrum or the emrep. Owing to the rescaling used in constructing the profiles, the distribution of contributions around the maximum value of λ_h is not a simple Gaussian function. However, the emreps do readily enable one to identify the general pattern of the contributions of the high-frequency distortion modes to the overall reorganizational energy as is evident by examination of Figures 2 and 5.

The emreps show significant contributions to the reorganizational energy that arise at about 400−800, 1500−2000, 2100−2700, and 2800−3200 cm^{-1} (regions 1, 2, 3, and 4 in Figure 2c). These regions correspond to the frequencies of the metal−ligand skeletal vibrations, the NH_2 deformations (or N−H stretch), and C≡N stretch, N−D stretch, and N−H stretch.

The observed absorption and emission spectra, the deconvoluted fundamental components, and the principal reorganizational energy contributions to the emission spectra are summarized in Table 1.

The contributions of the C≡N stretch are of particular interest. They are displayed most clearly in the emreps based on emission spectra obtained in butyronitrile solutions and for the deuterated (ND) complexes (Figure 5). Based on these contributions, we can evaluate the magnitude of λ_{CN}. The values of the emreps at $h\nu_x = 2000$ cm^{-1} are nearly identical for the NH and ND isotopomers, and there are no significant corrections for the vibronic contributions of the N−D stretch or the NH_2 deformation at this vibrational frequency. Second order contributions from the lower frequency vibrational modes probably do make a significant contribution. An estimate of this contribution can be based on (λ_{1000}^2/1000); since the value of λ_x at $h\nu_x = 1000$ cm^{-1} must be the result of the superposition of several vibronic

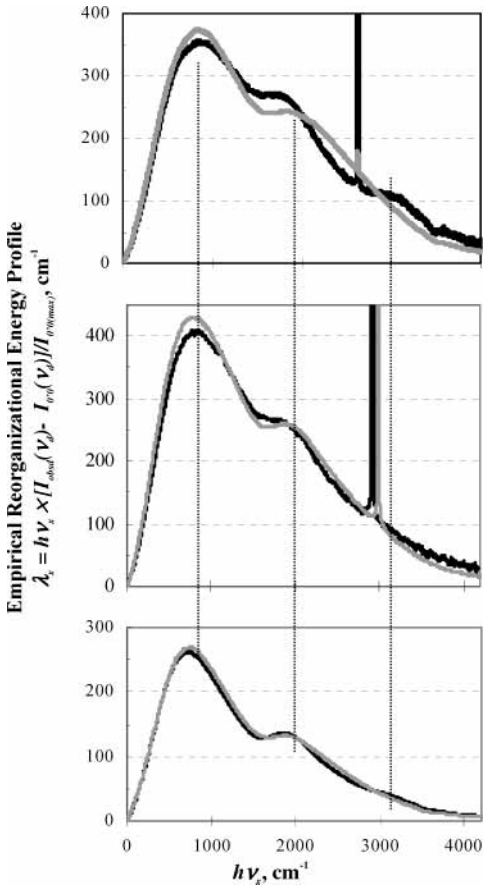

Figure 5. Empirical reorganizational energy profiles of $[Cr([14]aneN_4)(CNRu(NH_3)_5)_2]^{5+}$ (black curves) and $[Cr(d_4\text{-}[14]aneN_4)(CNRu(ND_3)_5)_2]^{5+}$ (gray curves) in DMSO/water (top), in the microcrystalline solid (middle) and in butyronitrile (bottom). Vertical lines are drawn for $\nu_x \approx 650$, 2000, and 3000 cm^{-1} to facilitate comparisons of the general regions of the metal−ligand stretching, C≡N stretching and N−H stretching vibrational modes.

contributions of slightly different frequencies, the actual second-order contributions may be smaller than this estimate. These values, averaged over the isotopomers, are 128 ± 6 cm^{-1} in DMSO/water, 52 ± 3 cm^{-1} in butyronitrile, and 155 ± 5 cm^{-1} in the solid. The corresponding values of λ_x are 240 ± 20, 130 ± 15, and 250 ± 30 cm^{-1} (uncertainties based on nm/pixel), and the values of λ_{CN} are greater than 108, 77, and 99 cm^{-1}, respectively.

The 77 K emission decay of this class of complexes is rarely fit by a single exponential, as has been noted previously.[1] The emission characteristics (lifetimes and spectra) are also excitation energy dependent. For excitation energies greater than the energy of the ambient MMCT absorption band maximum results in broadening on the high energy side of the emission band, and in one complex, we have been able to resolve the high energy emission component.[1,36,37] The high energy component (resolved for *trans*-$[Cr(ms\text{-}Me_6[14]aneN_4)(CNRu(NH_3)_5)_2]^{5+}$ with $h\nu_{max}(0'0) = 13\,800$ cm^{-1} and $\Delta\nu_{1/2}(0'0) = 210$ cm^{-1})[1,36,37] has the structured features associated with the metal centered $(^2E)Cr^{III}$ emission, and it is so assigned. We have used a two exponential fit for the decays reported here, and the amplitude weighted, average decay rate constants are reported in Table 1. Our previous work[1,37] has demonstrated that the MMCT and (^2E)-Cr^{III} excited states are very similar in energy (qualitatively illustrated in Figure 6) and that the higher energy $(^2E)Cr^{III}$ excited state has the longer lifetime in the ruthenated complexes (by a factor of 2 or more). The convolution of the decays of

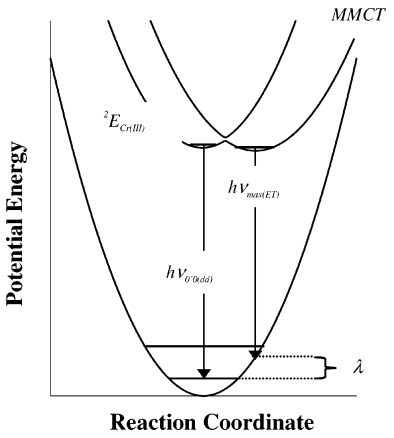

Figure 6. Qualitative PE curves illustrating the proximity and possible configurational mixing between the Cr^{III}-centered ^2E ligand field excited state and a Ru/Cr MMCT excited state of $[Cr([14]aneN_4)(CNRu(NH_3)_5)_2]^{5+}$.

the two excited states can be a source of the multiexponential decay behavior. Am(m)ine perdeuteration has a larger effect on the MMCT than on the $(^2E)Cr^{III}$ excited state of the tetraaza-macrocyclic complexes (for the parent $[Cr([14]aneN_4)(CN)_2]^+$ complex, $k_{NH}/k_{ND} = 8$ and $k_{NH}(77\ K) = 2.8 \times 10^3\ s^{-1}$);[1,37-42] it nearly eliminates the $(^2E)Cr^{III}$ component from the observed MMCT spectrum even when high energy excitations are employed,[1,37] but it does not result in single-exponential decay of the perdeutero complexes. It is important to note that the emission spectra of $[Cr([14]aneN_4)(CNRu(NH_3)_5)_2]^{5+}$ and $[Cr(d_4\text{-}[14]aneN_4)(CNRu(ND_3)_5)_2]^{5+}$ reported here are not significantly different on their high energy sides; this indicates that the 532 nm excitations do not result in a significant population of the $(^2E)Cr^{III}$ excited state and that the decay rates and emission spectra stimulated by these long wavelength excitations should not be complicated by contributions of the $(^2E)Cr^{III}$ decay. A significant part of the complexity of the decays may arise from a distribution of solvation environments in the frozen solutions. The significantly smaller decay rate in butyronitrile than in water suggests that the decay is somewhat solvent dependent even in frozen solutions. However, the am(m)ine-polypyridyl complexes of ruthenium exhibit more nearly mono-exponential decay behavior in the same media.[43]

Discussion

We have used a calibrated InGaAs array detector and 532 nm laser excitation to obtain good quality (relatively high signal-to-noise), highly reproducible transition metal-to-transition metal emission spectra in the 750−1200 nm range for $[Cr([14]aneN_4)(CNRu(NH_3)_5)_2]^{5+}$ (and its perdeutero, ND, analog) at 77 K in frozen solutions and in the microcrystalline solid. The lifetime of this complex is about $^1/_{15}$ that of its perdeutero analogue in DMSO/water glasses and in the microcrystalline solid, and we have used the difference in the emission spectra of these complexes at $h\nu_x \sim 3000\ cm^{-1}$ from the emission maximum to evaluate the reorganizational energy, λ_{NH}, correlated with the N−H mediated nuclear tunneling pathway. The corresponding vibronic sidebands of the emission spectra are very weak: their intensities are proportional to $(\lambda_{NH}/h\nu_{NH})I_{0'0}$. To facilitate the evaluation of the N−H contributions to the emission spectra, we have constructed empirical reorganizational energy profiles that display the contributions of the distortion modes as the envelope of the sums of their reorganizational energy contributions (λ_x).The quantitative interpretation of contributions to the emission spectra or to the reorganizational energy envelopes is not simple for reasons described in the Results section. The evaluation of the individual distortion mode contributions requires some additional experimental information. To this end, we have used the differences in the reorganizational energy profiles for the proteo- and perdeutereo-am(m)ine complexes to evaluate the reorganizational energy contribution of the N−H stretching modes.

General Features of the MMCT Emission Spectra. The $\{e,0'\} \rightarrow \{g,0\}$ component of the $[Cr([14]aneN_4)(CNRu(NH_3)_5)_2]^{5+}$ emission is about 2000 cm^{-1} lower in energy than the fundamental component of the $(^2E)Cr^{III}$ emission of the dicyano parent.[1,36-38,40,44] The full width at half-height of the fundamental component of the emission is 710 ± 30 cm^{-1} at 77 K in DMSO/H_2O glasses, comparable to that of $[Ru(bpy)_3]^{2+}$ (680 cm^{-1}) and slightly smaller than that of $[Ru(NH_3)_4bpy]^{2+}$ (1200 cm^{-1}) determined under the same conditions.[36,43,45] For comparison, the observed bandwidths (all determined in DMSO/H_2O glasses as described in this report) of the $(^2E)Cr^{III}$ emission components of $[Cr([14]aneN_4)(CN)_2]^+$ are about 75 cm^{-1} at 77 K in DMSO/H_2O[38,40] and that of the $\{e,0'\}\rightarrow\{g,0\}$ component of the resolved $(^2E)Cr^{III}$ emission that results from 437 nm excitations of $[Cr(ms\text{-}Me_6[14]aneN_4)(CNRu(NH_3)_5)_2]^{5+}$ is 210 cm^{-1}.[36,37] The observed emission spectra are broadened on their low energy sides by weak vibronic contributions.

General Features of the emreps for $[Cr([14]aneN_4)(CNRu(NH_3)_5)_2]^{5+}$. The emreps indicate that the dominant contributions to the differences in the electron-transfer excited state and ground-state geometries of this complex are vibrational modes in the 400−800 cm^{-1} region. Owing to the much greater intensity of the fundamental in much of this region, the amplitudes of the profiles are very uncertain in this region.[36] Nevertheless, it is clear that the excited state distortion is largely a result of displacements in vibrational modes in the metal−ligand stretching region,[35,46] consistent with the large differences in bond lengths expected between Cr(II) and Cr(III) in the respective electronic states. The largest values of λ_x are small: if the displacement is in a single mode averaged over all six Cr-ligand bonds with a mean force constant of $f \cong 100\ N\ m^{-1}$ and for $\lambda_x = 6 \times {}^1/_2 f\Delta Q_x^2$, then ΔQ_x is about 5 pm per Cr-ligand bond. The breadth of the largest reorganizational component of Figure 2c suggests that several vibrations contribute to the distortion (see results section) and that distortion in any specific bond length (or angle) is probably very small. Substantial bond-length changes are expected for the formation of high spin Cr^{II} from Cr^{III} (increases of ~33 pm each for two axial and ~7 pm each for four equatorial bonds to water),[29,47,48] so these small metal−ligand distortions are more consistent with the $d\pi^4$ low spin (triplet) than the $d\sigma d\pi^3$ high spin (quintet) Cr^{II} center in the MMCT excited state.

A puzzling feature of the emreps in Figure 5 is that the contributions to λ_x in the metal−ligand stretching region are about 50% larger in the solid and in DMSO/water than in butyronitrile (Table 1). This suggests that there are solvent induced differences in the molecular excited-state distortions. This could be a consequence of differences in the mixing of the $(^2E)Cr^{III}$ and the MMCT excited states since their relative energies and separation along the configuration coordinate will be solvent dependent, but the resolution of this will have to await further studies.

There is a prominent shoulder in the 1600−2300 cm^{-1} region of all of the reorganizational energy profiles generated for this complex. Some of this arises from overlap with the NH_2 deformation (see below), but the better resolved shoulder in the deutereo (ND) complexes is consistent with a substantial

reorganizational energy contribution from the cyanide stretch. Earlier work on the CN-bridged donor/acceptor complexes has shown that the C≡N stretch is strongly entangled with the electronic coupling,[5,6,27,28,49−51] and resonance-Raman studies of the MMCT absorptions of some related $[(NH_3)_5MNCM'(CN)_5]^-$ complexes have implicated distortions in the CN stretching modes,[21,52−54] so some contribution of these modes might be anticipated. The principal additional contribution in this region arises from second-order contributions of lower energy vibronic components (see comments in the Results section), and these are probably less than 150 cm^{-1}. This suggests that $\lambda_{CN} > 100$ cm^{-1}. There are two cyanides in the $[Cr([14]aneN_4)(CNRu(NH_3)_5)_2]^{5+}$ complex. Since the coupling between the terminal ruthenium centers is very weak,[50,51] the hole is probably localized at one of these centers, and one cyanide bridges the excited state donor−acceptor pair and the other does not. There is no way to know whether only one or both cyanides contribute to λ_{CN}. Similarly, the resolution is not adequate to distinguish between the contributions of the symmetric and the antisymmetric combinations of the C≡N stretches (the observations on the ground state indicate that there is a strong symmetry constraint on this vibronic coupling).[27,49]

The differences in the profiles of the proteo- and perdeutero-am(m)ine complexes in the $\nu_x = 1400-1800$ cm^{-1} region implicate a significant contribution of the NH_2 bending mode to the reorganizational energy: maximum differences of emreps of the proteo (NH) and deutero (ND) complexes at about 1560 and 1644 cm^{-1} in DMSO/water and butyronitrile, respectively. This was unexpected. There is some indication of a contribution from the M−N−H rocking modes (700−1100 cm^{-1}), but the uncertainties are large compared to the differences in the emreps of the proteo- and perdeutero-am(m)ine complexes in this region.

High-Frequency N−H Stretching Modes. The difference between the emreps of $[Cr([14]aneN_4)(CNRu(NH_3)_5)_2]^{5+}$ and $[Cr(d_4\text{-}[14]aneN_4)(CNRu(ND_3)_5)_2]^{5+}$, Figure 2d, clearly exhibits the contributions of NH stretching vibrational modes at ∼3200 cm^{-1}. This contribution is present in all the spectra (Figure 5) but best defined in DMSO/water solutions (trace amounts of H_2O could exchange with ND and diminish the amplitude of the contributions in butyronitrile or the solid). From the amplitudes of the contributions in DMSO/H_2O and DMSO/D_2O, we infer that $\lambda_{NH} \cong 28 \pm 5$ cm^{-1}. This is less than 10% of the contributions of the metal−ligand stretching modes to the reorganizational energy, and hence to the excited-state distortion.

Contributions to Emission Bandwidths. The substantial bandwidths inferred for the emission band components in 77 K frozen solutions ($k_BT \cong 53$ cm^{-1}) could be the result of several contributions. Some low frequency skeletal vibrations in these complexes, especially those that correspond to bending and deformation modes, have frequencies smaller than 200 cm^{-1} (∼$4k_BT$) and would contribute to the bandwidth. A distribution of environments (different arrangements of solvent molecules; contributions from surface and bulk species in the very fine solid particles) of the complex ion can also result in broadened spectra. The low-frequency skeletal vibrations and any solvent modes that are not frozen in 77 K glasses will contribute to the bandwidth as λ_l in eq 6. Finally, any distortion modes with vibrational frequencies that are less than the intrinsic bandwidth of the fundamental will be at least partially convoluted into the bandwidth in our analysis. That the emission bandwidths are larger in frozen solution than in the microcrystalline solid indicates that there are solvent contributions to the bandwidth. One interpretation of the similar mean decay lifetimes found in DMSO/H_2O and the microcrystalline solid is that the solvent modes correlated to electron-transfer are frozen in the solution. The appreciably smaller decay rate constant in butyronitrile may indicate some contribution of unfrozen solvent modes in this solvent. In any event, it appears that the solvent contribution to the overall reorganizational energy is small for the conditions of our experiments.

NH Mediated Excited-State Electron-Transfer: Nuclear Tunneling Pathways. That the excited state lifetimes of the Cr(CN)Ru complexes are on the order of a microsecond or longer strongly suggests that the excited state back electron-transfer process is spin forbidden; note that these lifetimes are roughly comparable to those of $[Ru(bpy)_3]^{2+}$ (the deutereo, ND, complex has a longer lifetime, the proteo complex a shorter lifetime), a complex with a comparable ground state CT absorptivity per chromophore. This inference is supported by some features of the vibronic structure, noted above, and that only "spin-forbidden" transition metal excited state-to-ground-state relaxation processes have been observed.[55,56] It is convenient to consider the nonradiative, excited-state electron-transfer rate constant in the form[10]

$$k_{nr}^0 \xleftarrow{T\to 0} \kappa_{el}\kappa_{nu}\nu_{eff} \xrightarrow{0 \ll T} k_{nr}(T) \tag{12}$$

The Franck−Condon contributions to the rate constant are contained in κ_{nu}, ν_{eff} is the nuclear frequency near the surface crossing point, and the electronic transmission coefficient, κ_{el}, is different from unity only when H_{eg} is small (as in a spin forbidden process).

We do not find a significant difference in zero-point energies of the deutereo and proteo complexes so the isotope effects most likely arise from nuclear tunneling mediated by the NH stretching modes. The large observed (in DMSO/water) isotope effect, $k_{NH}/k_{ND} \sim 15$, and the small value of $\lambda_{NH} \sim 27$ cm^{-1} are qualitatively consistent with a dominant nuclear tunneling pathway for the relaxation of the electron-transfer excited state. In the simple harmonic oscillator limit that only a single high-frequency vibrational mode mediates the relaxation, and for $\kappa_{el} \ll 1$[14]

$$k_{nr}^0 = H_{eg}{}^2\left[\frac{8\pi^3}{h^3\nu_h E_{ge}^{0'0}}\right]^{1/2} e^{(-\gamma_h E_{ge}{}^{0'0}/h\nu_h)} \tag{13}$$

$$\gamma_h = \ln(E_{ge}^{0'0}/\lambda_h) - 1 \tag{14}$$

Substitution of $\lambda_h \cong 27$ cm^{-1} and $h\nu_h \cong 3200$ cm^{-1} into eq 13 leads to $k_{nr}^0 \sim 0.5H_{eg}{}^2$ s^{-1}. Although $H_{ge} \cong 3200$ cm^{-1} has been estimated for the spin-allowed configurational mixing of the ground state of this complex with the[4] MMCT excited state,[28] the above result (and eq 13) can only be correct if H_{eg} is no more than a few percent of this value. As an illustrative example, $H_{eg} \sim 200$ cm^{-1} is about the largest value for which eq 13 would be approximately correct (note that we have no direct experimental measure of H_{eg}), and a value of this magnitude would lead to $k_{nr}^0 \sim 10^4$ s^{-1}, or an order of magnitude or so smaller than the observed value. Spin−orbit coupling is appreciable for transition metal complexes[57] and a value of H_{eg} could be of the order of the value cited, since the differences in energy between the configurationally similar excited states (E_{DQ} for excited MMCT doublet and quartet states) are not large (values for the energy difference between Ru^{II}-bpy singlet and triplet MLCT excited states have been estimated to be in the range of 1000−4000 cm^{-1});[22,58,59] for H_{SO}, the spin−orbit coupling matrix element, $H_{eg} \approx (H_{SO}/E_{DQ})H_{ge}$. It appears that an NH-mediated tunneling pathway as evaluated based on eq 13 and the observed

reorganizational parameters somewhat underestimates the observed rate constant.

A fit of the observations to a mechanism involving both tunneling in high-frequency modes and thermal reorganization in some low-frequency modes[13,60] gives similar results. Assuming a very small contribution of λ_l, a small value of H_{eg}, with the relaxation rate constant given by eqs 3−4, $G_j = (E_{ge}^{0'0} - \lambda_l - j h\nu_h)$ and an appropriate expression is[13]

$$k_{nr}(T) = \frac{2\pi^2}{h}\frac{{H_{ge}}^2}{(\pi\lambda_l k_B T)^{1/2}}(FC) \qquad (15)$$

Since k_BT and λ_l are so small, j and λ_l have to be chosen so that $G_j \cong 0$ in order fit the observation that $k_{nr} \sim 10^6\ s^{-1}$. The maximum value ($G_j = 0$) estimated from eq 15 is $k_{nr}(T) \sim 2{H_{ge}}^2$. This is not significantly different, considering the uncertainties, from the estimate based on eq 13, but it may be in a little better agreement with the observed decay rates.

Both of these estimates, and eqs 13 and 15, are based on two state, simple harmonic oscillator models, and these models do not represent well the complexities of the present system. The emitting MMCT excited state and the near in energy (^{2}E)-Cr^{III} excited-state amount to a mixed valence pair, and if they have the same spin multiplicity, there could be appreciable configurational mixing between them (see Figure 6). This configurational mixing would tend to flatten the excited-state potential energy surface, thereby increase the vibrational overlap with the ground state and result in a value of k_{nr} that is significantly larger than estimated by either of these equations. Consequently, the estimates above should be taken as lower limits of the tunneling rate constants.

The very small, but finite value of λ_{NH} does imply that the isotope effect, k_{NH}/k_{ND}, will be very large for the NH-mediated tunneling pathway. For example, eq 13 implies that $k_{NH}/k_{ND} \geq 500$. That the observed value is smaller is not surprising for the reasons noted above, but the tendency of k_{NH}/k_{ND} to increase with the number of NH moieties[1] suggests a degeneracy effect that would only be important if some other low temperature relaxation channels were competitive with ND-mediated tunneling. The larger reorganizational energy inferred for the cyanide stretch and eq 13 imply that a C≡N-mediated tunneling pathway could be 50 times more favorable than the ND-mediated pathway.

Conclusions

We have detected vibronic sidebands attributable to the N−H stretching modes in the near-infrared electron-transfer emission spectrum of a simple transition metal complex by means of a careful comparison of the emission spectra of the complex and its am(m)ine perdeuterated analogue. To make the high-frequency contributions more evident, we have rescaled the emission spectral data to obtain an empirical reorganizational energy profile. The amplitudes of the contributions to this profile are functions of reorganizational energies associated with the vibronic components and the corresponding displacement modes. The reorganizational energy components attributable to the N−H stretching modes are very small, consistent with a N−H mediated nuclear tunneling mechanism for the back electron-transfer relaxation of the excited state and with the very large isotope effects. The reorganizational energy contributions inferred from the emreps indicate that the largest excited-state distortions are in the metal−ligand skeletal stretching modes, consistent with the metal-to-metal nature of the excited state-ground-state transition. Substantial reorganizational energy contributions from a bridging ligand (C≡N) stretching mode and resolvable contributions from NH_2 bending modes are also inferred from the emreps.

Acknowledgment. The authors thank the Office of Basic Energy Sciences of the Department of Energy for partial support of this research.

Appendix A.

Generation of Empirical Reorganizational Energy Profiles (emreps) from Emission Spectra. 1. The emission spectrum is represented as the sum over some sets of vibronic progressions (the components of a progression are designated by subscript j; different vibronic progressions by a subscript h) as in eqs 2−5.[9,19,30,32]

2. To facilitate the evaluation of the different vibronic contributions, the fundamental is subtracted from the emission spectrum and the energy scale is defined by the energy difference from the fundamental (i.e., set $h\nu_{max}$(fundamental) = 0; all manipulations of data in EXCEL). A typical difference spectrum is shown in Figure 2b.

3. To generate a representation in which the relative contributions of different vibrational modes to the excited state distortion are graphically displayed, both the intensity and energy axes must be rescaled and corrected.

a. Equation 1 is a consequence of eqs 2−5 for the ratio of (FC) when $j = 1$ and $j = 0$ for a given high-frequency vibronic component h when $\lambda_h < h\nu_h$. The rescaling of the intensity axis is based on eq 1.[9,30] To emphasize the relative contributions to excited-state distortion, eq 1 may be rearranged to obtain a spectrum or profile of reorganizational energy contributions from the different vibronic components by multiplying the difference between the observed and the fundamental-component intensity at each energy by $h\nu_d/I_{0'0(max)} = [h\nu_{obsd} - h\nu_{0'0}]/I_{0'0(max)}$; for this purpose, the vertical axis is approximately $h\nu_d[I_{obsd}(\nu_d) - I_{0'0}(\nu_d)]/I_{0'0}(\nu_{0'0(max)})$ where $I_{0'0}(\nu_d)$ is the intensity of the fundamental at the frequency ν_d, $I_{obsd}(\nu_d)$ is the observed emission intensity, and $I_{0'0}(\nu_{0'0(max)})$ is the intensity of the fundamental at its maximum.

b. The correction of the energy axis is necessary because the vibronic components in the emission spectrum of this complex have significant bandwidths (equal to that of the fundamental), and this, combined with the rescaling of the intensity axis, results in displaced maxima of these vibronic components.

An approximate correction can be accomplished by the following procedure: For $h\nu_{vib(h)}$ the energy of the $0' \rightarrow 1$ vibrational transition of the hth ground-state high-frequency vibrational mode, each vibronic component is described by a Gaussian function of the form $I_{0'1}(h) = Ce^{-x^2/a^2}$, where C is a constant independent of emission energy, $x = [\nu_{0'0(max)} - \nu_h - \nu_{obsd}]$, and $a = \Delta\nu_{1/2}/2(\ln 2)^{1/2}$. The maximum of the first band of the hth vibronic progression occurs at $\nu_{obsd(m)} = [\nu_{0'0(max)} - \nu_h]$. The intensity scaling proposed above is equivalent to replacing the Gaussian functions by functions of the type

$$f = C(\nu_{0'0} - \nu_{obsd})e^{-x^2/a^2} \qquad (A1)$$

The maximum of this function with respect to $\nu_d = (\nu_{0'0} - \nu_{obsd})$ is given by

$$\frac{df}{d\nu_d} = Ce^{-x^2/a^2}[1 + 2\nu_{obsd(m)}\{\nu_h - \nu_{obsd(m)}\}/a^2] = 0 \qquad (A2)$$

Thus, in this representation of the data, the maxima of f are observed at

$$\nu_{\mathrm{obsd}(m)} = \frac{1}{2}\nu_h + \frac{1}{2}[\{\nu_h\}^2 + 2a^2]^{1/2} \qquad \text{(A3)}$$

Equation A3 can be rearranged and solved for ν_h. The direct solution contains a correction term, $a^2/\nu_{\mathrm{obsd}(m)}$, that is not useful for small values of $\nu_{\mathrm{obsd}(m)}$, but an inverse Taylor's expansion leads to a frequency parameter that more generally corresponds to the frequencies of the displacement modes

$$\nu_x = 2\nu_{\mathrm{d}} - [\{\nu_{\mathrm{d}}\}^2 + a^2]^{1/2} \qquad \text{(A4)}$$

Note that $a = \Delta\nu_{1/2}/2(\ln 2)^{1/2}$ is simply a number for each spectrum; the value of $\Delta\nu_{1/2}$ is the full width at half-maximum intensity obtained for the fundamental from the gaussian fit of the emission spectrum in the first step.

The use of $\nu_{\mathrm{d}} = (\nu_{0'0} - \nu_{\mathrm{obsd}})$ in rescaling the vertical axis in the reorganizational energy profile plots results in a related error of the amplitude of the maxima. This can be approximately corrected by substituting ν_x for ν_{d}. Thus, the final vertical axis is given by eq 7. The emreps are generated by plotting λ_x vs $h\nu_x$. This use of eqs A4 and 7 in scaling the axes amounts to a first-order iterative correction. Under some circumstances a higher order correction might be necessary. The correction terms are most important for small values of $h\nu_{\mathrm{d}}$. The uncertainties are intrinsically large in this regime since the amplitudes correspond to differences between two large numbers, $I_{0'0}(\nu_{\mathrm{d}})$ and $I_{\mathrm{obsd}}(\nu_{\mathrm{d}})$.

References and Notes

(1) Endicott, J. F.; McNamara, P. G.; Buranda, T.; Macatangay, A. V. *Coord. Chem. Rev.* **2000**, *208*, 61.
(2) Hush, N. S. *Prog. Inorg. Chem.* **1968**, *8*, 391.
(3) Marcus, R. A. *J. Phys. Chem.* **1990**, *94*, 4963.
(4) Gould, I. R.; Noukakis, D.; Luis, G.-J.; Young, R. H.; Goodman, J. L.; Farid, S. *Chem. Phys.* **1993**, *176*, 439.
(5) Endicott, J. F.; Watzky, M. A.; Macatangay, A. V.; Mazzetto, S. E.; Song, X.; Buranda, T. In *Electron and Ion Transfer in Condensed Media*; Kornyshev, A. A., Tosi, M., Ulstrup, J., Eds.; World Scientific: Singapore, 1997; p 139.
(6) Endicott, J. F.; Watzky, M. A.; Song, X.; Buranda, T. *Coord. Chem. Rev.* **1997**, *159*, 295.
(7) Marcus, R. A. *Discuss. Faraday Soc.* **1960**, *29*, 21.
(8) Marcus, R. A. *Annu. Rev. Phys. Chem.* **1964**, *15*, 155.
(9) Marcus, R. A. *J. Chem. Phys.* **1965**, *43*, 670.
(10) Newton, M. D.; Sutin, N. *Annu. Rev. Phys. Chem.* **1984**, *35*, 437.
(11) Newton, M. D. In *Electron-Transfer In Chemistry*; Balzani, V., Ed.; Wiley-VCH: Weinheim, Germany, 2001; Vol. 1, p 3.
(12) Newton, M. D. *J. Phys. Chem.* **1991**, *95*, 30.
(13) Kestner, N.; Logan, J.; Jortner, J. *J. Phys. Chem.* **1974**, *64*, 2148.
(14) Englman, R.; Jortner, J. *Mol. Phys.* **1970**, *18*, 145.
(15) Freed, K. F.; Jortner, J. *J. Chem. Phys.* **1970**, *52*, 6272.
(16) Kuznetsov, A. M.; Ulstrup, J. *Electron Transfer in Chemistry and Biology*; Wiley-VCH: New York, 1998.
(17) Matyushov, D. V.; Voth, G. A. In *Reviews in Computational Chemistry*; Lipkowitz, K. B., Boyd, D. B., Eds.; Wiley-VCH: New York, 2002; Vol. 18, p 147.
(18) Meyer, T. J.; Taube, H. In *Comprehensive Coordination Chemistry*; Wilkinson, G., Ed.; Pergamon: Oxford, U.K., 1987; Vol. 7, p 331.
(19) Barbara, P. F.; Meyer, T. J.; Ratner, M. *J. Phys. Chem.* **1996**, *100*, 13148.
(20) Lever, A. B. P. *Inorganic Electronic Spectroscopy*; Elsevier: Amsterdam, 1984.
(21) Hupp, J. T.; Williams, R. T. *Acc. Chem. Res.* **2001**, *34*, 808.
(22) Seneviratne, D. S.; Uddin, M. J.; Swayambunathan, V.; Schlegel, H. B.; Endicott, J. F. *Inorg. Chem.* **2002**, *41*, 1502.
(23) Solomon, E. I. *Comments Inorg. Chem.* **1984**, *3*, 227.
(24) Brunold, T. C.; Gudel, H. U. In *Inorganic Electronic Structure and Spectroscopy*; Solomon, E. I., Lever, A. B. P., Eds.; Wiley-Interscience: New York, 1999; Vol. 1, p 259.
(25) Birks, J. B. *Photophysics of Aromatic Molecules*; Wiley-Interscience: New York, 1970.
(26) Endicott, J. F.; Song, X.; Watzky, M. A.; Buranda, T. *Chem. Phys.* **1993**, *176*, 427.
(27) Watzky, M. A.; Endicott, J. F.; Song, X.; Lei, Y.; Macatangay, A. V. *Inorg. Chem.* **1996**, *35*, 3463.
(28) Watzky, M. A.; Macatangay, A. V.; Van Camp, R. A.; Mazzetto, S. E.; Song, X.; Endicott, J. F.; Buranda, T. *J. Phys. Chem.* **1997**, *101*, 8441.
(29) Endicott, J. F. In *Comprehensive Coordination Chemistry II*, 2 ed.; McCleverty, J., Meyer, T. J., Eds.; Pergamon: Oxford, U.K., 2003; Vol. 7, p 657.
(30) Endicott, J. F. In *Electron Transfer in Chemistry*; Balzani, V., Ed.; Wiley-VCH: New York, 2001; Vol. 1, p 238.
(31) Myers, A. B. *Acc. Chem. Res.* **1998**, *30*, 5519.
(32) Mulliken, R. S.; Person, W. B. *Molecular Complexes*; Wiley-Interscience: New York, 1967.
(33) Hush, N. S. *Electrochim. Acta* **1968**, *13*, 1005.
(34) Loring, R. F. *J. Phys. Chem.* **1990**, *94*, 513.
(35) Nakamoto, K. *Infrared and Raman Spectra of Inorganic and Coordination Compounds. Part B*; Wiley: New York, 1997.
(36) Chen, J. Y.; Xie, P.; Uddin, M. J.; Endicott, J. F. *Inorg. Chem.* submitted.
(37) McNamara, P. G., Ph.D. Dissertation, Wayne State University, 2000.
(38) Ryu, C. K.; Lessard, R. B.; Lynch, D.; Endicott, J. F. *J. Phys. Chem.* **1989**, *93*, 1752.
(39) Lessard, R. B.; Endicott, J. F.; Perkovic, M. W.; Ochrymowycz, L. A. *Inorg. Chem.* **1989**, *28*, 2574.
(40) Lessard, R. B.; Heeg, M. J.; Buranda, T.; Perkovic, M. W.; Schwarz, C. L.; Rudong, Y.; Endicott, J. F. *Inorg. Chem.* **1992**, *31*, 3091.
(41) Endicott, J. F.; Perkovic, M. W.; Heeg, M. J.; Ryu, C. K.; Thompson, D. In *Electron Transfer in Inorganic and Bioinorganic Chemistry*; Isied, S. S., Ed.; American Chemical Society: Washington, DC, 1997; Vol. 273, p 199.
(42) Endicott, J. F.; Ramasami, T.; Tamilarasan, R.; Lessard, R. B.; Ryu, C. K.; Brubaker, G. B. *Coord. Chem. Rev.* **1987**, *77*, 1.
(43) Xie, P.; Chen, J. Y.; Uddin, M. J.; Endicott, J. F. work in progress.
(44) Ryu, C. K.; Wang, R.; Schmehl, R. H.; Ferrere, S.; Ludwikow, M.; Merkert, J. W.; Headford, L. E.; Elliott, C. M. *J. Am. Chem. Soc.* **1992**, *114*, 430.
(45) Xie, P.; Chen, Y.-J.; Endicott, J. F.; Uddin, M. J.; Senerivatne, D.; McNamara, P. G. *Inorg. Chem.* **2003**, *42*, 5040.
(46) Drago, R. S. *Physical Methods for Chemists*; Harcourt Brace Jovanovich: Orlando, FL, 1992.
(47) Sham, T. K. *Acc. Chem. Res.* **1986**, *19*, 99.
(48) Endicott, J. F.; Kumar, K.; Ramasami, T.; Rotzinger, F. P. *Progr. Inorg. Chem.* **1983**, *30*, 141.
(49) Macatangay, A. V.; Mazzetto, S. E.; Endicott, J. F. *Inorg. Chem.* **1999**, *38*, 5091.
(50) Macatangay, A. V.; Endicott, J. F. *Inorg. Chem.* **2000**, *39*, 437.
(51) Macatangay, A. V.; Song, X.; Endicott, J. F. *J. Phys. Chem.* **1998**, *102*, 7537.
(52) Doorn, S. K.; Hupp, J. T. *J. Am. Chem. Soc.* **1989**, *111*, 1142.
(53) Walker, I. C.; Palmer, M. H. *Chem. Phys.* **1991**, *153*, 169.
(54) Forlano, P.; Baraldo, L. M.; Olabe, J. A.; Della Vedova, C. O. *Inorg. Chim. Acta* **1994**, *223*, 37.
(55) Ferraudi, G. J. *Elements of Inorganic Photochemistry*; Wiley: New York, 1988.
(56) Endicott, J. F. In *Electronic Structure and Spectroscopy of Inorganic Compounds*; Solomon, E. I., Lever, A. B. P., Eds.; Wiley: New York, 1999; Vol. 2, p 291.
(57) Figgis, B. N.; Hitchman, M. A. *Ligand Field Theory and its Applications*; Wiley-VCH: New York, 2000.
(58) Lever, A. B. P.; Gorelsky, S. I. *Coord. Chem. Rev.* **2000**, *208*, 153.
(59) Endicott, J. F.; Schegel, H. B.; Uddin, M. J.; Senerivatne, D. *Coord. Chem. Rev.* **2002**, *229*, 95−106.
(60) Sutin, N. *Progr. Inorg. Chem.* **1983**, *30*, 441.